EXPERIMENTAL BEHAVIOUR AND MECHANICAL MODELLING OF DISSIPATIVE T-STUBS CONNECTIONS

M. Latour[1], G. Rizzano[2]

In this work, aiming to enhance the energy dissipation capacity of classical rectangular T-stubs, an hourglass shape is proposed for the T-stub flange according to the approach usually adopted for ADAS devices, and a new type of axial damper is developed. First, a mechanical model of the device is set up and a FEM model is carried out in ABAQUS code. The accuracy of both models is verified through comparison with experimental results. Next, on the basis of cyclic tests, the improvement of the energy dissipation capacity of classical T-stubs provided by the proposed approach is quantified and the low cycle fatigue curves are determined both with reference to the case of T-stubs on rigid support and of coupled T-stubs. The results of the work can represent a useful tool also for designing dissipative Double Split Tee Connection.

[1] University of Salerno, Civil Engineering Department, Salerno, Italy. Email address: mlatour@unisa.it

[2] University of Salerno, Civil Engineering Department, Salerno, Italy. Email address: g.rizzano@unisa.it

INTRODUCTION

Behavior of steel moment resisting frames under the seismic events occurred in last years evidenced a significant loss of resistance and ductility deriving from the premature fracture of welds. In fact, even though welded beam-to-column joints can be detailed to obtain full strength connections theoretically able to provide steel frames with adequate dissipation capacities, the difficulties deriving from the in situ manufacturing of the welds play a basic role leading often to a brittle behavior of the connections and, as a consequence, to an unsatisfactory behavior of the whole frame. From this point of view, bolted connections should be preferred in design of seismic–resistant steel frames provided that joints are designed to ensure the engagement in plastic range of beam ends rather than connections. The dissipation capacity of steel frames with bolted connections has already been investigated in order to verify the possibility of using this kind of frame as an alternative to welded moment frame (SAC, 2000; Leon & Swanson, 2000; Faella et al., 2000; Latour et al., 2008; Rizzano, 2006). In particular, with reference to Ductility Class High Frames (CEN, 2005b), a design criterion able to guarantee a full strength extended end-plate connections has already been proposed and validated by Piluso & Rizzano (2007) on the basis of a probabilistic analysis accounting for random material variability of the connecting elements, i.e. beam, column, end-plate, bolts.

As an alternative, the latest version of Eurocode 3 (CEN, 2005a) allows to design Steel Moment Resisting Frames with partial strength joints, provided that connecting elements possess adequate ductility and dissipation capacities under cyclic loads. Within this framework, some attempts to provide detailed rules for designing dissipative joints have already been proposed in technical literature (Fleischman & Hoskisson, 2000; Rizzano, 2006; Kim et al., 2007). This topic has also been investigated in previous works of the authors (Latour et al., 2008, Iannone et al., 2010), where an experimental program devoted to point out the behavior under cyclic loads of different joint typologies has been carried out. In particular, design criteria able to engage in plastic range specific joint components, in order to govern the joint dissipation capacity, and to assure a desired value of stiffness, strength and plastic rotation supply have been pointed out.

In recent years, a growing interest of the scientific community has been addressed to structural systems able to perform adequately during seismic events and, at the same time, easy to replace after the earthquake (Aiken et al., 1993b; Kelly, 1979). Within this framework the approach usually adopted consists on equipping the structure with supplemental damping devices able to dissipate a part of the seismic input energy reducing the seismic demand on the structural elements. Many works have been carried out in recent studies on this topic, leading to relevant results and to the development of a large number of high dissipation capacity dampers, either of friction or of yielding type (Aiken et al, 1993a; Constantinou et al., 1998; Christopoulos and Filiatrault, 2000; Kim et al., 2007).

In this paper, an innovative approach is followed. The advantages provided by the introduction in the structure of supplemental damping devices easy to be substituted after the earthquake are added to those typical of dissipative steel frames in which a large number of dissipative zones is expected at beam ends. This goal can be achieved designing partial strength joints and providing joints with ductile and simple replaceable elements. In addition, it is important to underline that in designing steel frames with global collapse mechanism the use of partial strength joints can lead to a significant reduction of the structural cost (Piluso et al., 1999). In fact, in many cases columns design is governed by the satisfaction of members' hierarchy criterion rather than by resistance and deformability checks. In Piluso et al., (1999), it has been demonstrated that the use of partial strength connections in frames designed to fail according to a global collapse mechanism, can lead to a reduction of the structural cost up to 25% in case of frames with long span and few storeys.

A partial strength joint typology particularly appropriate to this purpose is the Double Split Tee Connection in which the connecting elements are clearly identified and easily replaceable. The behavior of this type of connection is strictly related to that of a T-stub subjected to axial load, which models the top and bottom tee. In past, many scientific efforts have been devoted to understand and model the behavior of simple rectangular T-stubs under cyclic loads (Piluso and Rizzano, 2008). Such behavior, as pointed out in scientific literature, is affected by significant pinching due to many factors, such as the plastic deformation of bolts and contact phenomena. Moreover, the plastic mechanism of rectangular T-stubs is characterized by the concentration of plastic strain in two small areas of the flange corresponding to the flange-to-web connection and to the bolt axes. Such plastic mechanism concentrates strain demand in limited zones and, consequently, under cyclic loads quickly leads to the deterioration of stiffness, strength and energy dissipation capacity (Whittaker et al., 1989). Aiming to increase the energy dissipation capacity of T-stubs, in this work, starting from past experiences of the authors concerning monotonic and cyclic behavior of T-stubs (Piluso and Rizzano, 2008; Latour et al., 2011), concepts usually adopted for ADAS devices have been applied developing a dissipative T-stub.

This typology of damper can be easily used in beam-to-column joints in substitution of classic rectangular T-stub of Double Split Tee Connection.

MECHANICAL MODELLING OF THE DEVICE

In order to analyze the energy dissipation capacity of T-stub connections, the plastic behavior of classic rectangular T-stub should be preliminary considered. It is well known that three different failure mechanisms can arise depending on the ratio between the flexural strength of the flanges and the axial strength of the bolt (Faella et al, 1999). The most dissipative failure mechanism (type 1 mechanism) arises in case of strong bolt and weak flange. It is characterized by the formation of four plastic hinges in the T-stub flanges, two in correspondence of the bolts axes due to the bending moment caused by the prying force, and two located at the sections corresponding to the flange-to-web connection (Fig. 1).

In this case, the bending moment diagram along the flange of the T-stub is linear throughout the entire process of loading with two equal values of the moment at the section where the plastic hinges arise. It is clear that the classic rectangular shape of the T-stub flange doesn’t allow to engage the whole plate in plastic range because it yields only in the most stressed parts, i.e. the plastic hinge zones, confining the plastic deformations in finite regions. Therefore, the resulting curvature and strain demand is extremely high.

In order to increase the energy dissipation capacity of T-stub connections, it is easy to understand that an ideal X-shaped element subjected to a linear bending moment diagram yields along the whole plate extension providing plastic deformation and strain demand over the plate length (Fig. 2). This approach is mainly followed in the design of steel hysteretic dampers working in double curvature such as ADAS devices, which are elements usually adopted in combination with chevron bracing systems (Fig. 3). The shape of ADAS devices must differ from the ideal X shape, first of all because a proper dimension of the mid-section of the element is required to withstand axial and shear actions. In fact, in the modeling of such a kind of metallic dampers two effects should be considered: the moment-shear interaction and the catenary effects due to geometric non linearity. In particular, the latter effect, at high displacements, can lead to significant axial stresses in the plate and, as a consequence, to a reduction of the ductility supply.

For this reason, usually ADAS devices are characterized by the so-called "hourglass shape", whose geometry is defined by means of an exponential function. The mathematical formulations describing the ADAS devices shape have been empirically determined by Tena-Colunga (1996) starting from the results of tests carried out at the University of Berkeley by Whittaker et al. (1989). With reference to the notation of Fig. 2, the hourglass shape is described by the following exponential function (Tena-Colunga, 1996):

$$\begin{cases} b(z) = Be^{-\alpha \cdot z} & 0 \le z \le m/2 \\ b(z) = s \cdot e^{\alpha(z-m/2)} & m/2 \le z \le m \end{cases} \tag{1}$$

$$\alpha = \frac{2}{m} \ln\left(\frac{B}{s}\right) \tag{2}$$

where s is the width of the mid-section, B is the width of the clamped section and m is the distance between the sections stressed by the maximum level of bending moment which, in the case of T-stub, is represented by the distance between the bolt axis and the section corresponding to the flange-to-web fillet (Fig.1). This distance can be assumed, according to Eurocode 3 (CEN, 2005a), as $m=d-0.8r$, where d is the distance between the bolt axis and the face of the T-stub web and r is the radius of the flange-to-web connection in the case of rolled T-stub or $r=a_c\sqrt{2}$ in the case of welded T-stub with a_c equal to the weld throat thickness.

In order to model the force-displacement curve of a device with an hourglass shape the prediction of stiffness, resistance and ductility is required. Such prediction, for the complexity of the hourglass shape, is untrivial in a closed form solution. Hence, generally, simplified models are assumed to predict both the elastic behavior (initial stiffness) and the inelastic behavior (resistance and ductility).

Regarding the elastic behavior, initial stiffness of the hourglass T-stub can be evaluated following the same approach provided in Faella et al. (1996), where the stiffness of the T-stub is determined by means of a mechanical approach based on an equivalent cantilever model.

In particular, taking into account the width of the mid-section necessary to withstand the axial and shear actions, a simplified trapezoidal model has been adopted for the hourglass shape of the T-stub. Therefore, the ideal cantilever model of Fig.4, loaded by the bolt force, has been considered. The initial stiffness of the Hourglass T-stub ($K_{0,HS}$) has been determined and expressed by means of a formulation formally coincident with that of a simple rectangular T-stub. In particular, the following relationship has been obtained where ζ is a factor depending on the ratio between the width at the mid-section (s) and the width at the clamped section (B), and t is the thickness of the plate:

$$K_{0,HS} = \zeta \frac{EBt^3}{m^3} \tag{3}$$

where:

$$\begin{cases} \zeta = \dfrac{2(B-s)}{3B} \dfrac{4(B-s)^2}{4(B-s)A_1 + 4(B-s)A_2 - 2A_3} \\ A_1 = [(B-s) + (B-2s)\ln(B/s)] \\ A_2 = [(s-B) + B\ln(B/s)] \\ A_3 = [(3s-B)(B-s) + 2B(B-2s)\ln(B/s)] \end{cases} \tag{4}$$

The value of ζ corresponding to s/B=1 provides the well-known solution $\zeta = 0.5$ available for the T-stub with rectangular flange. Besides, considering s/B ratios adopted in tests of Whittaker et al. (1989), which vary from 0.1 to 0.2, the value of ζ ranges between 0.22 and 0.28 (Fig. 5). Therefore, for design purposes, the average value $\zeta = 0.25$ can be adopted.

Bolt pretension effects on the initial stiffness of the hourglass T-stub have been modeled according to the approach given in Faella et al. (1999). In particular, in this approach the influence of the preloading level on the degree of flexural constraint exhibited by the bolts is accounted for. On the basis of the analysis of experimental data, in Faella et al. (1999) this effect has been considered by properly correcting the formulation of the initial stiffness by means of a coefficient ψ depending on the ratio between the flexural stiffness of the flanges and the bolt axial stiffness. Therefore, in the case of preloaded bolts, the stiffness of the hourglass T-stub can be computed by replacing Eq. (3) with the following relationship:

$$K_{0,HS} = \psi\,\zeta\,\frac{EBt^3}{m^3} \qquad (5)$$

where ψ is given by (Faella et al., 1999, 2001):

$$\psi = 0.57\left(\frac{\mathrm{t}}{\mathrm{d_b}\,\sqrt{m/d_b}}\right)^{-1.28} \qquad (6)$$

with d_b equal to the bolt diameter.

Regarding the inelastic behaviour of the Hourglass T-stub, the prediction of the whole monotonic force-deflection curve can be performed by increasing step-by-step the bending moment level on the T-stub and assuming that the point of zero moment remains during the loading process located at the middle section between the bolt axis and the flange-to-web connection, according to the procedure already applied for rectangular T-stub in Piluso et al. (2001). Starting from the moment-curvature diagram of the cross-section, the displacement at the i-th loading step is evaluated by integrating the curvature along the plate and multiplying the obtained rotation for the distance *m*. Also in the prediction of the inelastic behavior a simplified model has been adopted in

this work. In particular, as already proposed by Whittaker et al. (1989), the largest X-shape inscribed within the real shape of the device is adopted (Fig.2). The effective width (B_{eff}) of the simplified bi-triangular X-shape has been determined starting from Eqs. (1) -(2) and imposing that tangent lines to the edges of the hourglass shape (axes *a* and *b* of Fig. 2) pass through the centre of symmetry (Point C of Fig. 2).
The following relationship has been determined:

$$B_{eff} = \frac{\alpha B m}{2} e^{\left(1-\frac{\alpha m}{2}\right)} \tag{7}$$

The evaluation of the force-displacement curve is significantly simplified in the case of X-shaped T-stub because, assuming an ideal linear shape, for each assigned moment distribution the curvatures are constant along the plate (Fig.2). Therefore, taking into account that the curvature χ_i corresponding to the i-th moment distribution can be expressed as a function of the strain ε_i of the extreme fiber ($\chi_i=2\varepsilon_i/t$), the following expressions have been obtained:

$$\delta_i = \frac{F_i}{K_{0,HS}} \qquad 0 \le \delta \le \delta_y \tag{8}$$

$$\delta_i = \frac{F_i}{K_{0,HS}} + \frac{(\varepsilon_i - \varepsilon_y) m^2}{t} \qquad \delta_y \le \delta \le \delta_u \tag{9}$$

where F_i, is the axial force acting on the T-stub which is defined, for a single T-stub with weak plate and strong bolts, by the following relation (fig. 1) (Faella et al., 1999):

$$F_i = \frac{4M_i}{m} \tag{10}$$

and ε_y is the yielding strain of the steel, δ_y is the displacement corresponding to the first yielding given by eq.(8) with $F_i=F_y$ and δ_u is given by eq.(9) for ε_i equal to the steel ultimate strain ε_u. F_y is given by:

$$F_y = \frac{4M_y}{m} = \frac{2}{3} \cdot \frac{B_{eff}\, t^2\, f_y}{\mathrm{m}} \qquad (11)$$

Eqs. (9), (10) and (11) allow to predict the whole inelastic branch of the F-δ curve of the hourglass T-stub up to failure.

EXPERIMENTAL PROGRAM

In order to verify the benefits provided by the proposed device in terms of energy dissipation capacity, an experimental program on rectangular and hourglass T-stubs under monotonic and cyclic loading conditions has been performed (Fig. 6).

Concepts of ADAS devices has already been applied to beam-to-column connections by Fleischman & Hoskisson (2000), where modular connectors produced as cast piece were proposed and analyzed. In this work, in order to simplify the manufacturing of the dissipative T-stub, ADAS concept is applied manufacturing the hourglass shape, by means of flame cutting, that is the main and easiest method for cutting steel. This technique even though provides cut surface with striated structure and some burring, minimizing the additional processing costs for the construction of the dissipative T-stubs can lead to advantageous structural solutions due to the reduction of the global cost as already underlined in Piluso et al. (1999).

The design of the tested specimens has been performed by using both the mechanical model above described and a Finite Element model carried out in ABAQUS code. In particular, with reference to the mechanical models, Eqs. (3)-(11) have been used in the case of hourglass T-stub, while the Piluso et al. model (2001) has been applied for designing the rectangular T-stubs.

Aiming to obtain a solid three-dimensional model the library element C3D8R, i.e. 8-node linear brick, with reduced integration and instability mesh control has been adopted. The choice of this type of element comes from the following considerations. First of all, aiming to reduce the computational effort, a first order element (linear brick) has been chosen, taking into account that, although second order element provide higher accuracy than the first order element, in presence of complicated phenomena, such as contacts and slips, the computational effort exponentially grow. In addition, in order to reduce the processing time, a "reduced integration element", using a lower order integration to form the element stiffness, has been adopted. In case of eight node bricks, integration points are reduced from eight to one. In this way, element assembly is approximately eight times less costly compared to the case of full-integration elements. This choice does not reduce accuracy of the analysis provided that an instability mesh control is simultaneously applied.

Full integration elements may undergo shear and volumetric locking due to their numerical formulation, which gives rise to shear strains that do not really exist, while reduced integration elements can exhibit the mesh instability phenomena often known as hourglassing (Maenchen & Sack, 1964; Kosloff & Frazier, 1978). This is a special case of the phenomenon known in finite elements as kinematic modes or spurious zero-energy modes. Practically, since the elements have only one integration point, it is possible for them to distort in such a way that the strains calculated at the integration point are all zero which, in turn, leads to uncontrolled distortion of the mesh. In order to control this phenomenon the viscous approach of ABAQUS code has been employed in the FE modeling. The effects due to the axial stiffness of the plate and to the catenary actions arising at large displacements have been accounted for by means of a static non-linear analysis. The geometric non linearity has been properly accounted for to grasp the full post elastic behavior of tested T-stubs, which are characterized, at large displacements, by considerable second order effects. To this scope, the stiffness matrix is formulated considering the current configuration of the nodal position. Furthermore, in FE model, the interactions between the plates and between hole and bolt have been modeled by means of a frictionless formulation and the bolt pretension effect has been modeled by imposing, in a preliminary loading step, an appropriate thermal distortion.

As already underlined, an experimental analysis has been planned to verify the possibility to increase the energy dissipation capacity under cyclic loads of T-stubs by adopting an hourglass shape. The purpose of the study has been comparative. In fact, basic idea was to show that rectangular and hourglass T-stubs can be properly designed in order to obtain the same monotonic force-displacement response, i.e. same stiffness and resistance, but different dissipative behaviors under cyclic loads.

To this goal, by applying a trial and error procedure the following design conditions have been imposed:

– the initial stiffness of the hourglass T-stub $K_{0,\mathrm{HS}}$ is equal to that of the corresponding T-stub with rectangular flange;
– the energy dissipation capacity of the hourglass T-stub is maximized by properly cutting the T-stub flanges;
– the inelastic branch of the F-δ curve of hourglass T-stub fits that of the corresponding rectangular T-stub up to its ultimate displacement.

In order to achieve the design goals, within the design process, the following three geometrical parameters have been considered: the distance *m* between the bolt and the plastic hinge, the width of the plate *B*, and the thickness of the plate *t*. These three parameters have been chosen as main design parameters because they strongly affect the T-stub overall behavior and, in particular, initial stiffness, resistance and the ductility. In fact, as already examined in Faella et al, (1999), the initial stiffness is related to the ratio $(B\,t^3)/m^3$, the plastic resistance corresponding to the knee of the force-displacement curve of the T-stub depends mainly on the parameter $(B\,t^2/m)$ and the ductility is governed by the parameter m^2/t. It is clear that the reduction of the section width along the plate due to the hourglass shape leads mainly to a reduction of the T-stub stiffness which can be recovered by increasing width *B* and thickness *t* and reducing the distance *m*. The simultaneous respect of the three previous design condition provided the most appropriate combination of values of the three geometrical design parameters.

The whole experimental program consists of 21 welded T-stub specimens, 11 with rectangular plates and 10 with hourglass plates. The elements have been connected through the flanges by means of four M18 bolts of 8.8 class (CEN,2005a) with a preloading level l equal to 80% of the yield stress. Two type of steel grade have been used: S275 and S355 (CEN, 2005c).

The specimens are divided into two series. The first one is constituted by twelve specimens which have been realized connecting the T-stubs to a rigid and strong flange. Four specimens have been tested under monotonic load and eight under constant amplitude cyclic loads. The second series is composed by nine specimens constituted by two equal T-elements. Also in this case both monotonic tests (two specimens) and cyclic tests (seven specimens) have been performed.

The identity tag of the specimens allows identifying all the examined cases. After symbol TS, which is the abbreviation of T-Stub, the presence or absence of letter D (Double) differentiates specimens of the second series (Coupled T-stubs) from the elements of the first series (T-stubs on rigid support). Symbol –XS, which is the acronym of X-Shaped, identifies hourglass T-stubs. Finally, symbols –M or –C individuate, respectively, monotonic tests and cyclic tests. Moreover, with reference to cyclic tests, after letter C, constant cyclic amplitude is also specified.

The values of the geometrical properties of the specimens are given in Table 1, with reference to symbols of Fig. 5.

The goal of cyclic tests under different constant amplitudes was the evaluation of the low cycle fatigue curves, in order to compare the dissipative capacities of the X-shaped elements with respect to the rectangular ones. The experimental tests were carried out at the Materials and Structures Laboratory of the Department of Civil Engineering of Salerno University. All the specimens were subjected to a tensile axial force, applied under displacement control to the webs by the jaws of the testing machine, a Schenck Hydropuls S56 (maximum test load 630 kN, piston stroke ±125 mm). Monotonic tested were executed by applying the tensile load at speed of ±0.01 mm/s. The same speed has been adopted in cyclic tests, which have been executed under displacement control adopting a triangular waveform. Each cyclic test is characterized by a sequence of tensile loading up to the cyclic displacement amplitude, unloading and compressive loading up to the zero displacement.

In addition, coupon tensile tests have been performed to establish the mechanical properties of the material. The values of the mechanical properties are given in Table 1.

MONOTONIC TEST RESULTS AND MODEL VALIDATION

T-stubs on rigid support (TS01-M, TS02-M, TS01-XS-M, TS02-XS-M)

The experimental tests (Figs.8-9) on T-stubs connected to rigid support evidenced a good reliability of the design procedure previously described. Monotonic tests show that the experimental curves of the hourglass T-stub are close to that of the rectangular ones

(Figs.10-11). In addition, it can be observed that monotonic behavior is significantly influenced by the axial forces due to the presence of the rigid support which represents a shear constraint for the bolts. This effect is greatest in the case of T-stub connected to a very rigid support. In fact, during the loading process, T-stub deforms while the rigid support remains in elastic range, not exhibiting significant deformations. Therefore, in this case, shear actions on the bolt become prevalent and significant axial force arises in the fastened plate (Fig.12a). On the contrary, in the case of two equal T-stubs connected through the flanges, during the loading process the bolt axes follows the flange deformation and therefore shear actions in bolts are negligible (Fig.12b).

Failure of specimens TS01-M, TS02-M, TS01-XS-M and TS02-XS-M was caused by axial stresses in the flange: in case of TS-M specimens bolt shear failure arose and in case of TS-XS-M specimens fracture of the hourglass mid-section occurred. Figs.13-14 show the comparisons between monotonic experimental curves and the predicted ones.

As already underlined, prediction of the F-δ curve has been computed by means of the model proposed by Piluso et al. (2001), for rectangular T-stubs. Conversely, the model previously derived has been applied for the hourglass T-stub.

It can be observed that both the mechanical model and the FE model provide a very accurate prediction of the monotonic behavior either for rectangular T-stub or for hourglass T-stub. Regarding the mechanical model, as it does not account for the influence of second order effects, it results sufficiently accurate only up to the T-stub displacement corresponding to the hardening branch due to the second order effects. Nevertheless, such approximation does not represent a problem, because this displacement is greater than the displacement expected from a structural point of view. In fact, it can be observed from Figs 10 and 11 that the second order effects became important for T-stub displacement greater than 20 mm. If we consider the T-stub as the element connecting the beam to the column in correspondence of the upper and lower flange of the beam (Double Split Tee Connection), the T-stub displacement equal to 20 mm provides a beam rotation equal to 0.05 rad and 0.04 rad for a beam depth equal to 400 mm and 500 mm respectively. These values are greater than the structural demand of the joint rotation capacity required by the codes. In fact, with reference to the Near Collapse limit state, Vision 2000 Report (SEAOC, 1995) provides a mean value equal to 0.025 rad, while Eurocode 8 (CEN, 2005b), for High Ductility Class, requires a minimum value of the plastic rotation supply of connections equal to 0.035 rad.

Coupled T-stubs (TSD-M, TSD-XS-M)

The experimental analysis on coupled rectangular T-stubs (Fig.15) and hourglass T-stubs (Fig.16) simulates the structural situation in which the thickness of the T-stub flange is similar to that of the support. Two monotonic tests TSD-M and TSD-XS-M have been performed on coupled T-stubs. The experimental results show a very ductile behavior (Figs.17-18). The comparison between the experimental results on T-stubs on rigid support and on coupled T-stubs shows that the influence of the axial forces in coupled T-stubs is significantly reduced with respect to that of T-stub on rigid support both with reference to rectangular T-stubs and to hourglass T-stubs. It can be recognized that the displacement corresponding to the increase of the slope of the hardening branch in the case of coupled T-stub is about 40 mm, which is approximately equal to two times that of the T-stub on rigid support. This is due, as already underlined, to the reduction of the shear restraining action exerted on T-stub bolts in the case of coupled T-stub.

In Figs. 17-18 the comparison between the Force-Displacement curves provided by the experimental tests and those obtained by means of mechanical modeling and FE models previously described is also shown. It can be observed, as already underlined with reference to T-stubs on rigid support, that the predictions provided by the mechanical models and FE model are very satisfactory and accurate in the range of interest. In particular, it can be observed that the FE model is able to accurately predict the force-displacement curve also in the range of high displacements because it accounts for the geometrical non-linearity. Conversely, the mechanical models, neglecting the influence of axial stresses, cannot be applied to the high displacement range which, as already underlined in the case of T-stub on rigid support, is not significant from a structural point of view.

CYCLIC TESTS AND ENERGY DISSIPATION CAPACITY IMPROVEMENT

T-stubs on rigid support (TS01-C, TS02-C, TS01-XS-C, TS02-XS-C)

Aiming to the analysis of low cycle fatigue, T-stubs have been subjected to constant amplitude cyclic tests. Regarding T-stub on rigid support, three cyclic tests under constant amplitude have been performed both for rectangular T-stub and for hourglass T-stub. The displacement amplitudes of the tests, equal for the three tests to 7.5, 15 and 22.5 mm (Figs.19-20), have been chosen aiming to cover a range of displacements significant for structural applications. In fact, as already underlined with reference to monotonic tests, the adopted maximum value of the T-stub displacement in cyclic tests equal to 22.5 mm leads to a joint rotation greater than the value of the rotation capacity required both by Vision 2000 Report (SEAOC, 1995) and by Eurocode 8 (CEN, 2005b).

All rectangular T-stubs exhibit the same failure mode regardless of the imposed displacement amplitude. Cracking of flanges initially developed at welds and progressively propagated along the flange width and thickness up to the complete fracture of the flange, which produced the complete loss of the load-carrying capacity. The behavior gave rise to a progressive deterioration, up to failure, of axial strength, stiffness and energy dissipation capacity, as shown in Figs. (19-20).

The hourglass T-stubs showed the same failure mode characterized by the complete fracture of the flange. Moreover, cyclic behaviors of hourglass T-stubs are very different compared to that of rectangular T-stubs in terms of spread of plasticity and, as a consequence, of energy dissipation capacity.

This is firstly confirmed by the experimental evidence provided by the monitoring of the specimens during the test by means of thermal camera (Fig.21). The measurement of the heat on the T-stub flanges during the second cycle both for rectangular and hourglass T-stub confirms the expected mechanism of plasticization of the metal. In fact, in the case of rectangular T-stub, a significant gradient of temperature has been measured along the flange confirming the concentration of the energy dissipation in correspondence of the bolts and of the flange-to-web connection (Fig.21b). In the case of the hourglass element the diffusion of the plasticization is evidenced by the reported shot, which shows a uniform thermal state in the whole flange (Fig.21a).

In order to completely and quantitatively point out the different plastic behavior under cyclic loads of the two details, the low cycle fatigue curves have been carried out. To this scope, it is preliminary necessary to establish the conventional collapse condition, as there is no universally recognized failure criterion. Generally, in scientific literature collapse condition is identified in correspondence of a given value α of the degradation of strength, stiffness or energy dissipation capacity. In this work the failure condition has been identified checking the degradation of Energy Dissipation Capacity, because it is able to account for the overall behavior of the T-stubs, including also the reduction of stiffness and strength. According to Castiglioni and Calado (1996), the value α=0.5 has been assumed as the conventional level of deterioration corresponding to failure. In particular it is assumed that the collapse is reached when the condition $E_i/E_1=0.5$ is satisfied, where E_i is the energy dissipated during the i-th cycle and E_1 is the corresponding value recorded during the first cycle (Fig.22). First of all, it has been observed that in all cyclic tests the hourglass T-stub attained the collapse after a number of cycles much higher than that provided by rectangular T-stub. As shown, for example, in Fig. 22 with reference to cyclic tests under constant amplitude of 15 mm, the number of cycles to conventional failure of hourglass T-stub is equal to 149 instead of 11 of rectangular T-stub.

The low cycle fatigue curves, as well known, can be represented by means of straight lines in bi-logarithmic scales. The number of plastic reversal to failure N_f is related to the total displacement amplitude Δv by means of the following relationship:

$$\Delta v = a N_f^b \tag{12}$$

on the base of the results of cyclic tests under different values of constant amplitude displacement (Fig.22) low-cycle fatigue curves have been defined evaluating through least square fitting parameters *a* and *b*. First of all, it can be observed that, in the examined case, the monotonic points are not well aligned with the low-cycle fatigue curves. This behavior is related to the different failure mechanisms occurring under cyclic and monotonic loading. In fact in the case of cyclic tests, as the cyclic amplitudes are contained in a displacement range in which second order effects do not have relevance, the failure of the element is due to the fracture of the plate while in the case of monotonic tests, as above underlined, the constraining action of the rigid support caused the premature shear failure of the bolt. The low cycle fatigue curves depicted in

Fig.23 show the significant improvement of the energy dissipation capacity provided by the hourglass T-stub. The ratio between the energy dissipated up to the conventional failure by hourglass T-stub and by the rectangular T-stub is equal, on the average, to 7.5. As the two curves are characterized by the same slope and the curve of hourglass T-stub is above that of the rectangular T-stub, the enhancement in terms of number of cycles up to failure is significant in the whole range of the investigated cyclic displacement amplitudes resulting always greater than 650%.

Coupled T-stubs (TSD, TSD-XS)

The results of cyclic tests on coupled rectangular and hourglass T-stubs are depicted in Fig.24, which confirm that also in the case of coupled T-stubs the enhancement of the device response under cyclic loading conditions is very significant.

In Fig.25 low-cycle fatigue curves of rectangular and hourglass T-Stubs are depicted. Even in this case, the monotonic points are not well aligned with the curves obtained by means of regression analysis of the three cyclic points. As already underlined with reference to T-stubs on rigid support, this behavior arises because in the cyclic tests the second order effects do not have relevance, so that the failure modes under cyclic and monotonic conditions are different. The comparison between the low-cycle fatigue curve of the rectangular T-stubs and that of the hourglass T-stubs shows the significant increase of the energy dissipation capacity obtained by properly cutting the T-stub flanges also in the case of coupled T-stubs. In particular, the ratio between the energy dissipated up to failure of hourglass and rectangular T-stub is equal, on the average, to 2.8.

Finally, Figs.23 and 25 evidence that low cycle fatigue curves in the cases of rigid support and coupled elements are characterized by the same slope which is approximately equal to 0.5. The intersection of low cycle fatigue curves with the vertical axis is almost the same in the case of rectangular element while, in the case of the hourglass T-stub, a higher value is shown by T-stubs on rigid support. This testifies that the benefit provided by the hourglass configuration in terms of energy dissipation capacity increases as far as the thickness of the connected plate increases.

CONCLUSIONS

In this paper, an approach to improve the energy dissipation capacity of bolted T-stubs under cyclic loads has been analyzed by means of a theoretical and experimental analysis whose results can be summarized as follows:

- the hourglass shape of the T-stub flanges, whose geometry is defined by means of the relationships usually applied to ADAS devices, is able to spread the plasticity along the entire flange avoiding premature fracture of the middle section for bending and shear, as confirmed by the results of tests and by the specimen observation through thermal camera;
- a mechanical model for predicting the whole force displacement curve of the hourglass T-stub has been developed. The comparison with experimental monotonic tests executed both on rectangular and hourglass T-stubs showed the accuracy of the model in predicting the initial stiffness and the whole force-displacement curve up to T-stub displacements corresponding to joint rotations greater than 0.04 rad, which can be considered as typical values for structural applications;
- the finite element modeling developed in ABAQUS code provided a very accurate prediction of the entire monotonic force displacement curve up to failure of both rectangular and hourglass T-stub;
- the improvement of the plastic behavior under cyclic loads provided by hourglass T-stub has been quantitatively pointed out by means of cyclic tests under constant amplitude which showed that the ratio between the energy dissipated up to the conventional failure by hourglass T-stub and by the rectangular T-stub is equal, on the average, to 7.5 for T-stubs on rigid support and to 2.8 for coupled T-stubs;
- the low cycle fatigue curves in the cases of T-stub on rigid support and coupled elements are characterized by the same slope, approximately equal to 0.5, while the benefit provided by the hourglass configuration in terms of number of cycles up to failure and, therefore, in terms of energy dissipation capacity, is greater for T-stubs on rigid support with respect to that of coupled T-subs, highlighting that this benefit increases as far as the thickness of the plate connected to the T-stub increases.

It is important to underline that the results of the work can represent useful tools also for designing dissipative beam-to-column joint such as Double Split Tee Connection.

REFERENCES

Aiken ID, Nims DK, Whittaker AS, Kelly JM, 1993a. Testing of Passive Energy Dissipation Systems.*Earthquake Spectra, Vol.9, no.3.*

Aiken ID, Clark PW, Kelly JM, 1993b. Design and Ultimate-Level Earthquake Tests of a ½.5 Scale Base-Isolated Reinforced-Concrete Building. *Proceedings of ATC-17-1 Seminar on seismic Isolation, Passive Energy Dissipation and Active Control. San Francisco. California.*

CEN, 2005a. Eurocode 3: Design of Steel Structures. Part 1-8 Design of Joints. *European committee for standardization.*

CEN, 2005b. Eurocode 8: Design of Structures for Earthquake Resistance. Part 1: General rules, rules for buildings and seismic actions. *European committee for standardization.*

CEN, 2005c. Eurocode 3: Design of Steel Structures. Part 1-1: General Rules and Rules for Buildings. *European committee for standardization.*

Christopoulos C, Filiatrault A, 2000. Principles of Passive Supplemental Damping and Seismic Isolation. *IUSS PRESS. Pavia. Italy*

Constantinou M.C., Soong T.T., Dargush, G.F., 1998. Passive Energy Dissipation Systems for Structural Design and Retrofit. *Multidisciplinary Center for Earthquake Engineering Research, University at Buffalo, State of New York.*

Faella C., Piluso V., Rizzano G. 2000. Structural Semi-rigid Connections – Theory, Design and Software. *Boca Raton, Ann Arbor, London, Tokyo: CRC Press*

Fleischman R., Hoskisson B. 2000. Modular connectors for seismic resistant steel moment frames 2000. *Proceedings of Structures Congress 2000, Philadelphia, PA, May 7-10.*

Kelly JM, 1979. Aseismic Base Isolation: A review. Proceedings, 2nd U.S. National Conference on Earthquake Engineering, Stanford, CA, 823-837

Kim Y, Oh S., Ryu H., Kang C. 2007. Hysteretic behaviour of moment connections with energy absorption elements at beam bottom flanges. *ICAS 2007, Oxford.*

Kosloff D., Frazie G.A. 1978. Treatment of hourglass patterns in low order finite element codes. *International Journal for Numerical and Analytical Methods in Geomechanics. Vol.2, pp.57-72.*

Iannone F., Latour M., Piluso V., Rizzano G. 2010. Experimental Analysis of Bolted Steel Beam-to-Column Connections: Component Identification. In print in Journal of Earthquake Engineering.

Latour M., Piluso V., Rizzano G. 2008. Cyclic model of beam-to-column joints. *5th European Conference on Steel and Composite Structures, EUROSTEEL 2008, 3-5 September 2008, Graz, Austria. Brussels: ECCS.*

Leon R., Swanson A. 2000. Cyclic modelling of T-stub connections. *Proceedings of steel structures in Seismic Areas, Canadaù*

Maenchen, G., Sack, S. 1964. The Tensor Code. *Methods in Computational Physics, Vol.3, pp.181-210.*

Piluso V., Rizzano G. 2008. Experimental analysis and modelling of bolted T-stubs under cyclic loads. *Journal of constructional steel research, vol.64, pp.655-669*

Piluso V., Rizzano G. 2007. Random material variability effects on full-strength end-plate beam-to-column joints. *Journal of constructional steel research, vol.63*

Piluso V., Faella C., Rizzano G. 2001. Ultimate behavior of bolted T-Stubs. I: Theoretical model. *Journal of Structural Engineering ASCE, vol.127, n°6, pp.686-693*

Rizzano G. 2006. Seismic design of steel frames with partial strength joints. *Journal of earthquake engineering, vol.10, n°5*

SAC, 2000. Recommended Design Criteria for New Steel Moment Resisting Frames Buildings, *California*.

SEAOC 1995. (Structural Engineers Association of California). Performance Based Seismic Engineering of Buildings, *Vol. I, Part1: Interim Recommendations, Part2: Conceptual Framework; April 1995.*

Tena-Colunga A.. 1997. Mathematical modelling of the ADAS energy dissipation device. *Engineering Structures, vol.19, n°10, pp. 811-821.*

Whittaker A., Bertero V., Alonso J., Thompson C. 1989. Earthquake simulator testing of steel plate added damping and stiffness elements. *UCB/EERC-89/02*

LIST OF FIGURES AND TABLES

Figure 1. Failure modes of bolted T-stubs

Figure 2. Definition of the geometry, curvature and bending moment diagrams

Figure 3. Frames with ADAS devices

Figure 4 Simplified model for the stiffness prediction

Figure 5 Correlation between the ζ factor and the ratio *s/B*

Figure 6. Typologies of the tested specimens

Figure 7. Finite Element Model of the hourglass T-stub

Figure 8: Experimental test on hourglass T-stub on rigid support

Figure 9: Experimental test on rectangular T-stub on rigid support

Figure 10: TS01-M vs TS01-XS-M: monotonic tests comparison

Figure 11: TS02-M vs TS02-XS-M: monotonic tests comparison

Figure 12: Deformed shape of T-stub on rigid support and coupled T-stubs

Figure 13: Rectangular T-stub Model Comparison

Figure 14: X-shaped T-stub Model Comparison

Figure 15: TSD series

Figure 16: TSD-XS series

Figure 17: TSD test result and models comparison

Figure 18: TSD-XS test result and models comparison

Figure 19: TS01-C and TS01-XS-C test results

Figure 20: TS02-C15 and TS02-XS-C15 test results

Figure 21: Propagation of the heat along the flange detected by thermal camera

Figure 22: Definition of the conventional collapse

Figure 23: TS and TS-XS low cycle fatigue curves

Figure 24: Cyclic test of the TSD-XS and TSD series

Figure 25: TSD and TSD-XS low cycle fatigue curves

TABLE 1- Specimens' geometry and steel mechanical properties

TABLE 2 - Energy Dissipated at Conventional Collapse

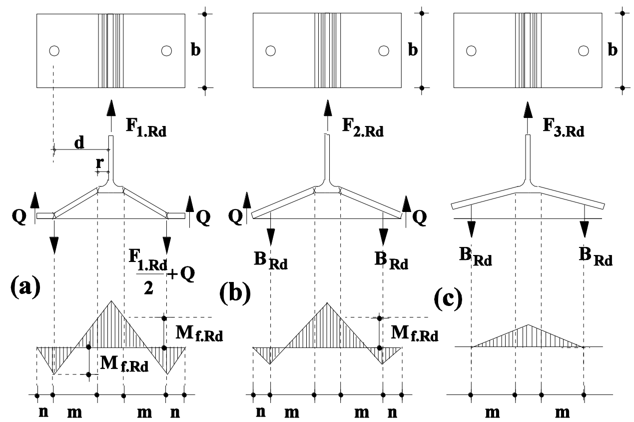

Figure 1. Failure modes of bolted T-stubs

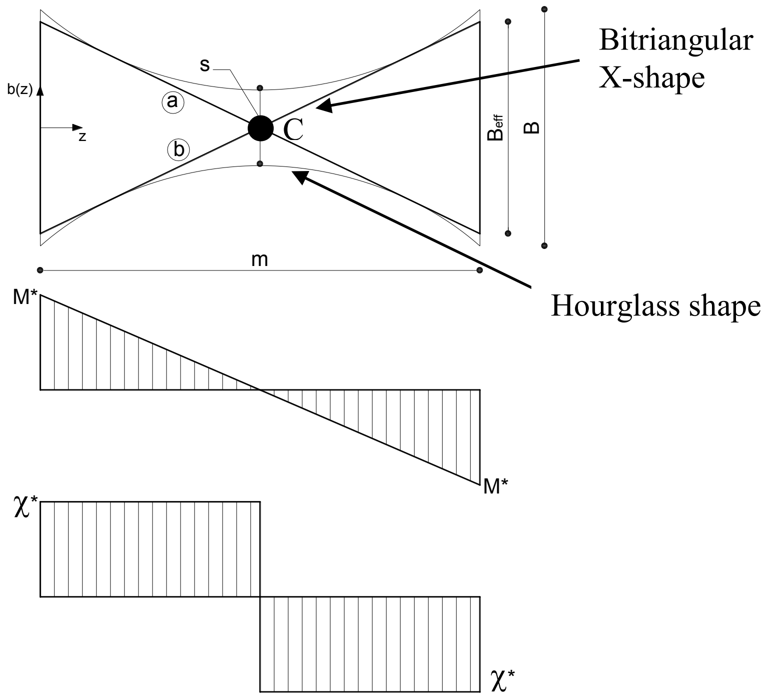

Figure 2. Definition of the geometry, curvature and bending moment diagrams

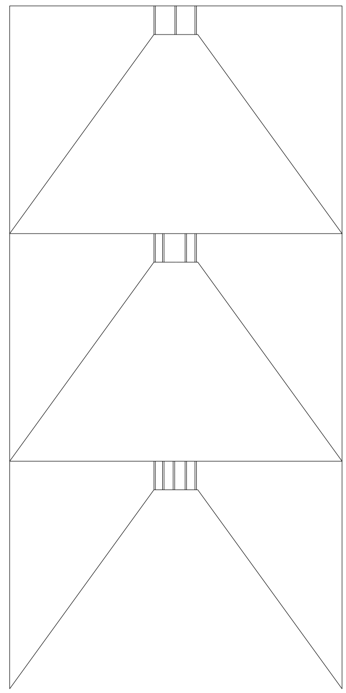

Figure 3. Frames with ADAS devices

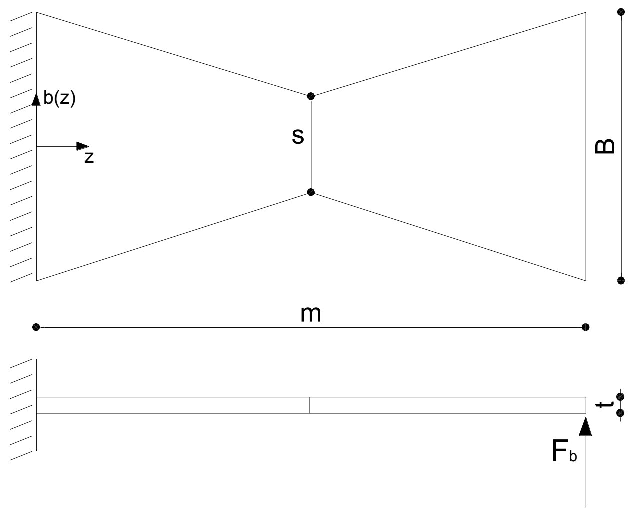

Figure 4 Simplified model for the stiffness prediction

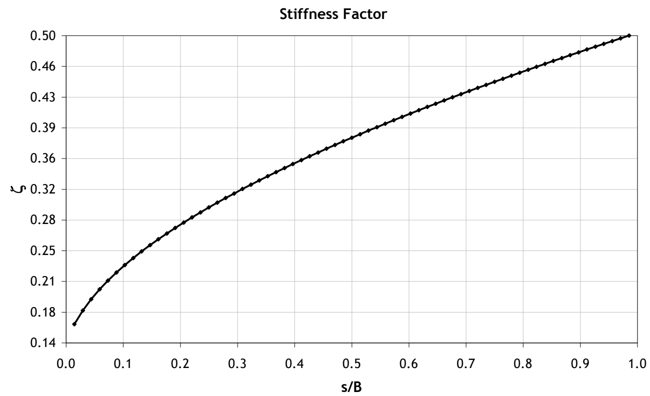

Figure 5 Correlation between the ζ factor and the ratio *s/B*

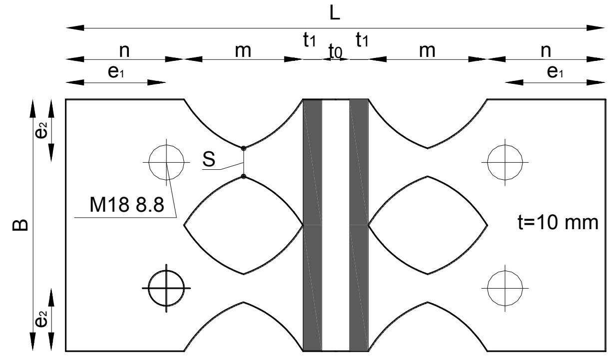

a) Hourglass T-stub

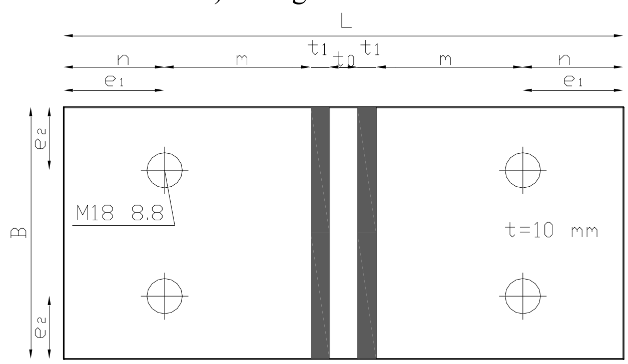

b) Rectangular T-stub

Figure 6. Typologies of the tested specimens

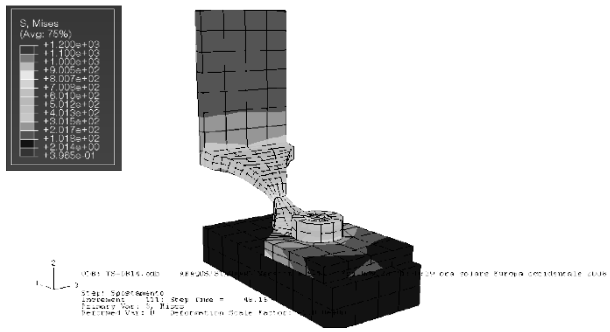

Figure 7. Finite Element Model of the hourglass T-stub

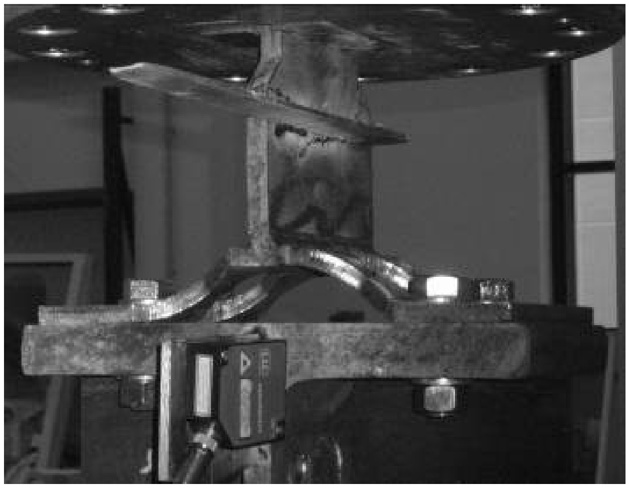

Figure 8: Experimental test on hourglass T-stub on rigid support

Figure 9: Experimental test on rectangular T-stub on rigid support

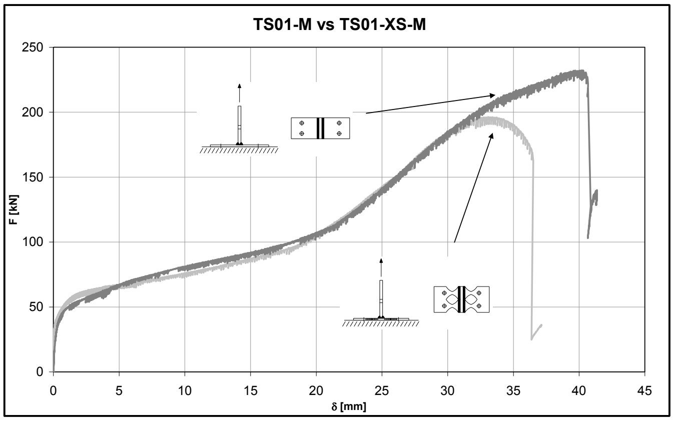

Figure 10: TS01-M vs TS01-XS-M: monotonic tests comparison

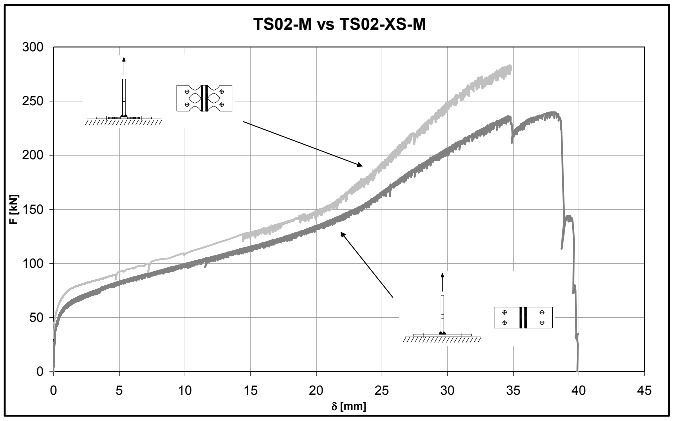

Figure 11: TS02-M vs TS02-XS-M: monotonic tests comparison

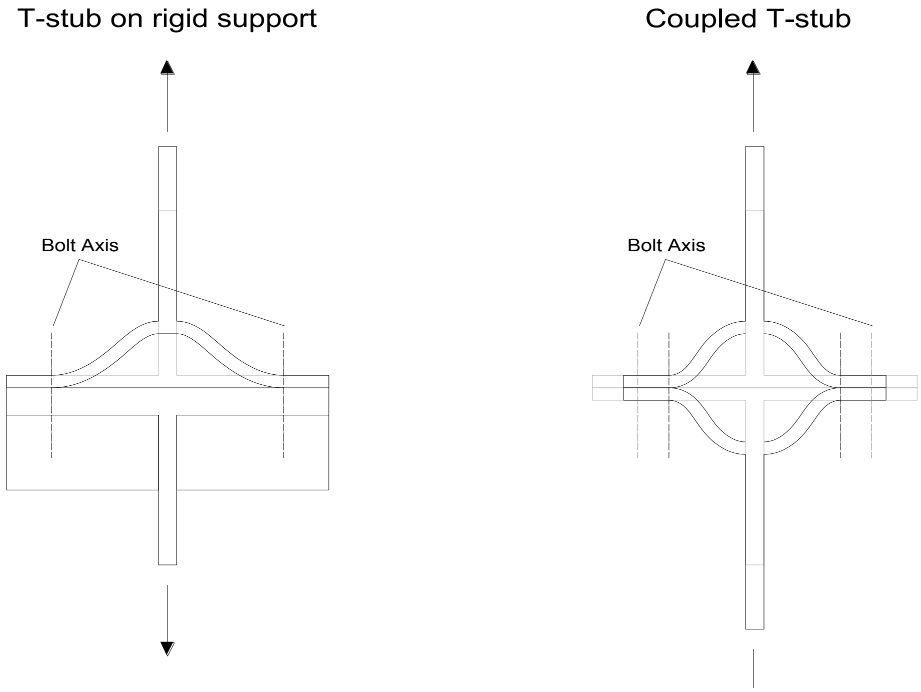

a) T-stub on rigid support b) Coupled T-stubs

Figure 12: Deformed shape of T-stub on rigid support and coupled T-stubs

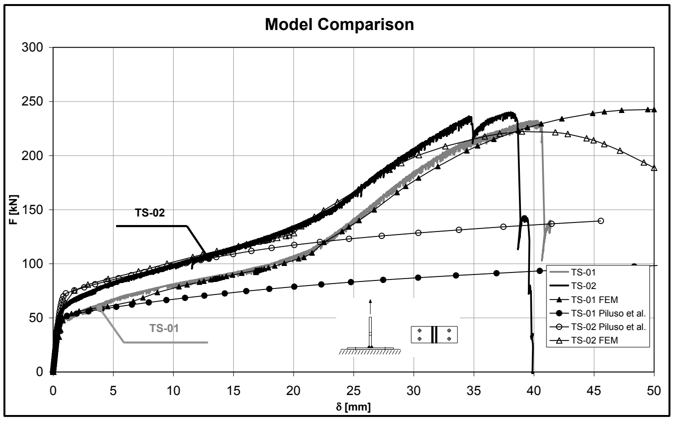

Figure 13: Rectangular T-stub Model Comparison

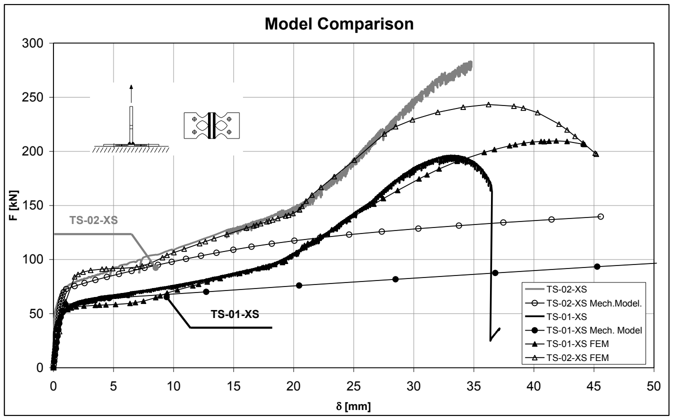

Figure 14: X-shaped T-stub Model Comparison

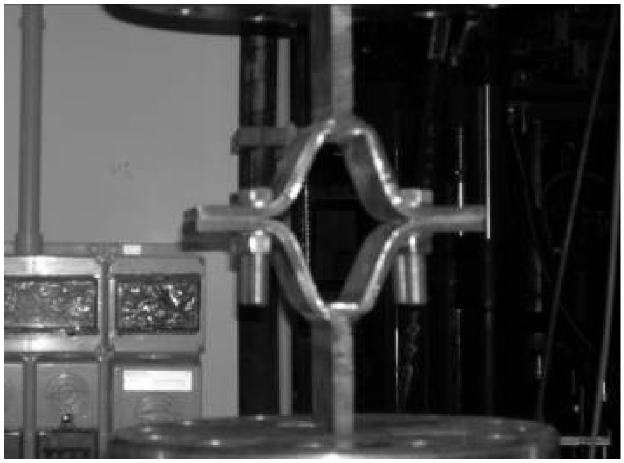

Figure 15: TSD series

Figure 16: TSD-XS series

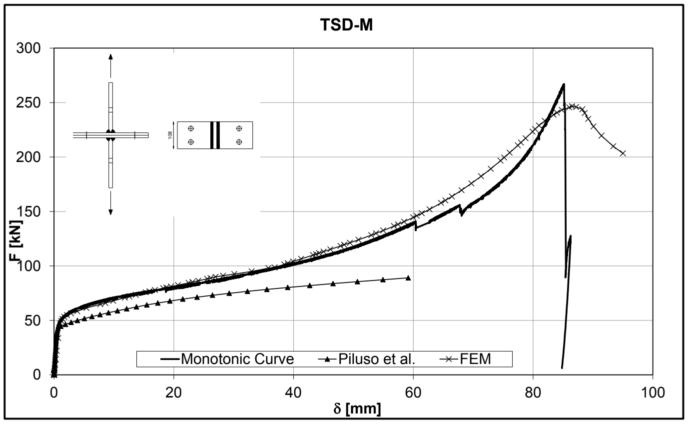

Figure 17: TSD test result and models comparison

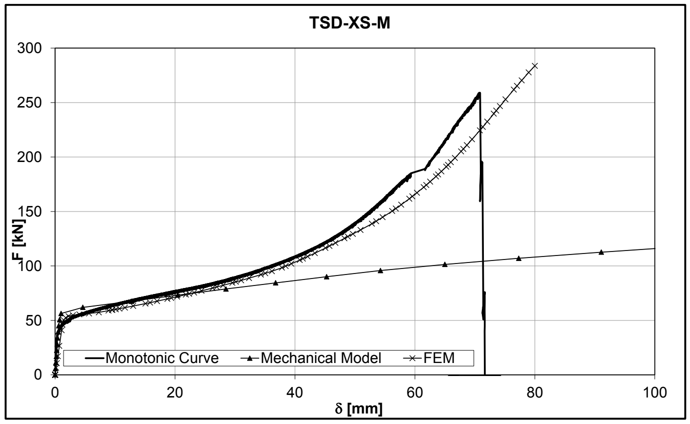

Figure 18: TSD-XS test result and models comparison

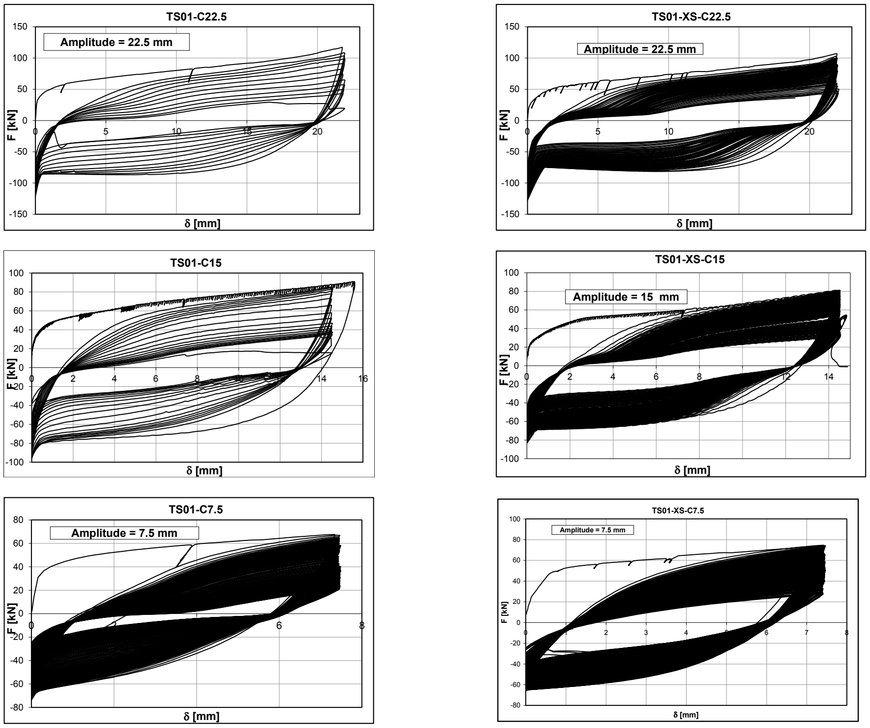

Figure 19: TS01-C and TS01-XS-C test results

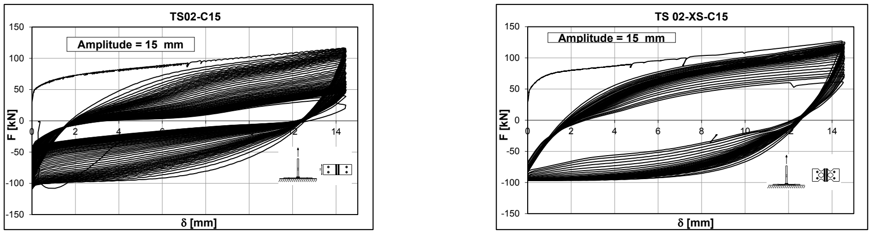

Figure 20: TS02-C15 and TS02-XS-C15 test results

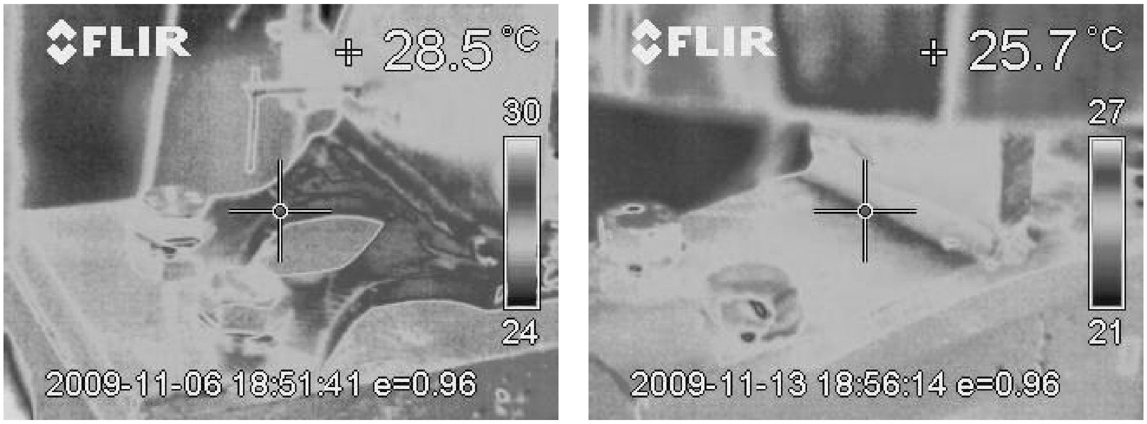

a) X-shaped T-stub b) Rectangular T-stub

Figure 21: Propagation of the heat along the flange detected by thermal camera

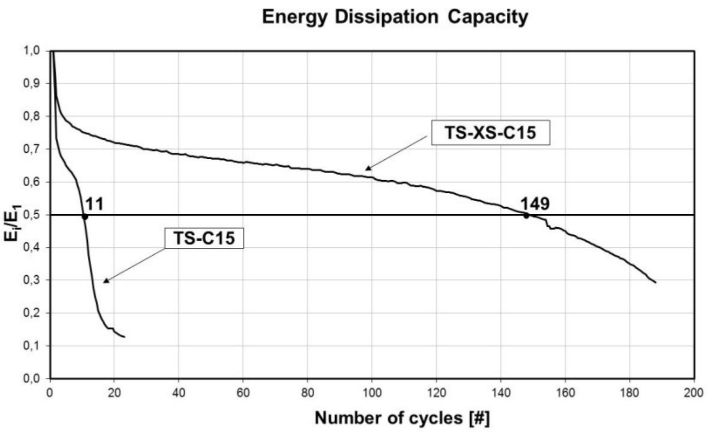

Figure 22: Definition of the conventional collapse

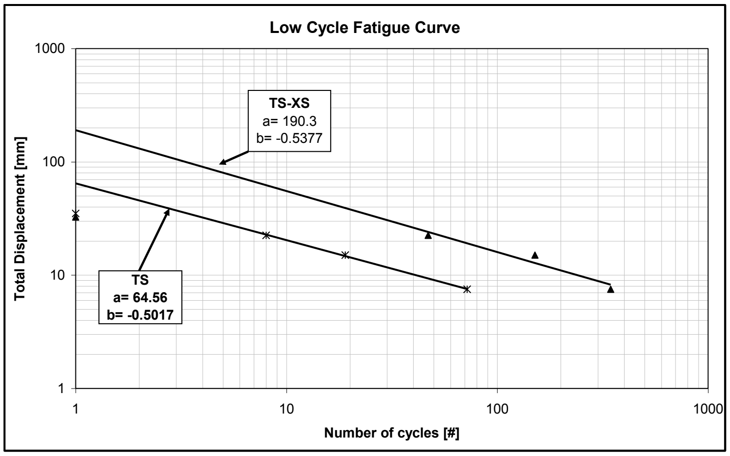

Figure 23: TS and TS-XS low cycle fatigue curves

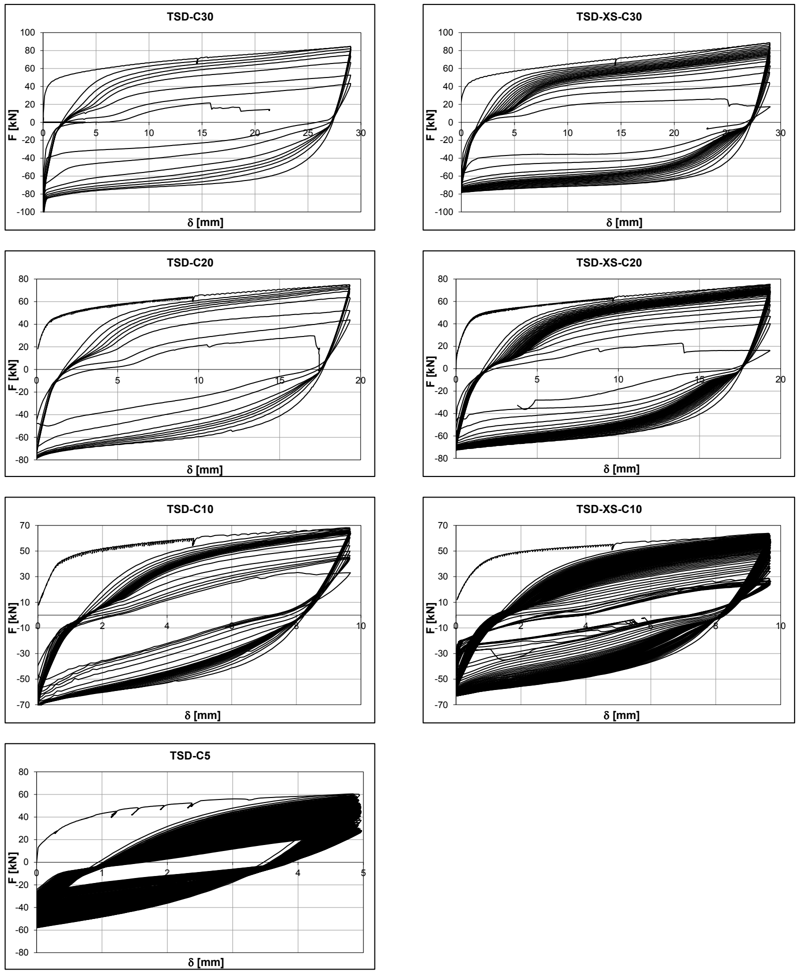

Figure 24: Cyclic test of the TSD-XS and TSD series

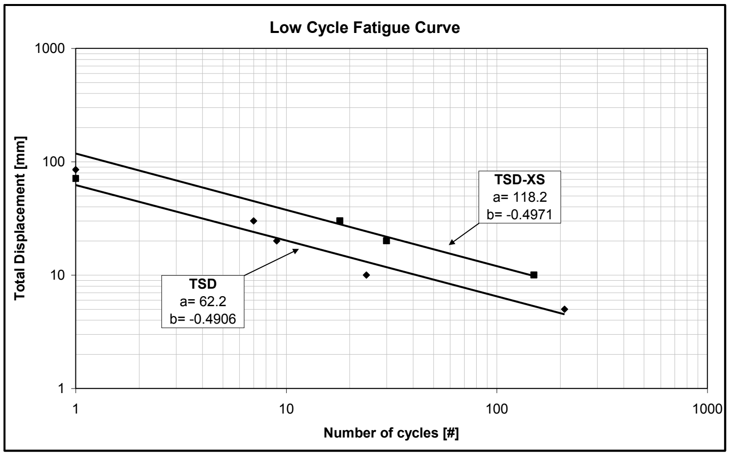

Figure 25: TSD and TSD-XS low cycle fatigue curves

TABLE 1

Specimens' geometry and steel mechanical properties

Specimen	n [mm]	m [mm]	s [mm]	t [mm]	t_1 [mm]	t_0 [mm]	B [mm]	e_1 [mm]	e_2 [mm]	f_y [MPa]	f_u [MPa]	ε_y [%]	ε_h [%]	ε_m [%]	ε_u [%]
TS01	54	80.5	-	10	10	15	108	54	20	272	441	0.13	1.87	9.88	45.3
TS02	54	80.5	-	10	10	15	108	54	20	391	626	0.18	2.37	7.4	40.8
TS01-XS	63.5	63.9	15.1	10	10	15	136	54	34	282	490	0.13	1.72	17.6	52.2
TS02-XS	63.5	63.9	15.1	10	10	15	136	54	34	456	663	0.18	2.37	8.5	66.4
TSD	54	80.5	-	10	10	15	108	54	20	272	441	0.13	1.87	9.88	45.3
TSD-XS	63.5	63.9	15.1	10	10	15	136	54	34	272	441	0.13	1.87	9.88	45.3

TABLE 2

Energy Dissipated at Conventional Collapse

Specimen	$E_{diss,cc}$ [kNm]	Specimen	$E_{diss,cc}$ [kNmm]
TS01-C7.5	24.4	TS01-C7.5	157.6
TS01-C15	14.7	TS01-C15	135.3
TS01-C22.5	17.6	TS01-C22.5	127.4
TSD-C5	74.8	-	
TSD-C10	14.8	TSD-XS-C10	40.8
TSD-C20	14.1	TSD-XS-C20	45.9
TSD-C30	20.1	TSD-XS-C30	48.8